Automatic Exposure Control in Pediatric and Adult Computed Tomography Examinations

Can We Estimate Organ and Effective Dose From Mean mAs Reduction?

Antonios E. Papadakis, PhD, Kostas Perisinakis, PhD,† Ismini Oikonomou, MSc,† and John Damilakis, PhD†*

Objectives: The purpose of this study was (i) to measure absorbed dose to radiosensitive organs and estimate the effective dose associated with fixed tube current and automatic exposure control (AEC)-activated standard computed tomography (CT) examinations, and (ii) to investigate the relationship between the average reduction of tube current achieved by AEC and the reduction in organ and effective dose.

Materials and Methods: Four physical anthropomorphic phantoms that represent the average individual as neonate, 1-year-old, 5-year-old, 10-year-old child, and the Rando phantom that simulates the average adult individual were employed. The phantoms were subjected to standard head and neck, thorax, and abdomen and pelvis scans using a 16-slice CT system. The scans were performed both with fixed tube current and with AEC. Dose measurements were performed for each scan using thermoluminescent dosimeters placed at internal locations in the phantoms and on the phantoms' surface. Dose measurements were performed for all radiosensitive organs according to the 2007 recommendations of the International Commission on Radiologic Protection. Effective dose was estimated on the basis of weighted sum of measured organ absorbed doses (ED_{MEAS}). Percent reduction of organ absorbed dose and effective dose were compared with the mean percent reduction of the tube current.

Results: The percent organ dose reduction achieved when AEC was activated in standard head and neck CT scans ranged from 26.6% to 42% for neonate, 8.1% to 63.8% for 1-year-old, −2.9% to 22.5% for 5-year-old, −8.7% to 44.9% for 10-year-old, and 16.3% to 50.1% for an adult. The corresponding values for thorax scans were found to range from −26.1% to 9.9% for neonate, −2.5% to 37.7% for 1-year-old, −20.8% to 15.4% for 5-year-old, −61.9% to 9.3% for 10-year-old, and 5.6% to 42.2% for an adult, whereas the corresponding values for abdomen and pelvis scans were found to range from −12.1% to 29.1% for neonate, −4.9% to 26.6% for 1-year-old, −11.7% to 38.9% for 5-year-old, −62.4% to −17.3% for 10-year-old, and 31.0% to 56.8% for an adult. In neonate, the ED_{MEAS} values ranged from 1.18 to 3.23 mSv for fixed tube current and 1.31 to 1.73 mSv for AEC scans. In 1-year-old phantom, the ED_{MEAS} values ranged from 1.71 to 2.82 mSv for fixed tube current and 0.99 to 2.38 mSv for AEC scans. In 5-year-old phantom, the ED_{MEAS} values ranged from 2.03 to 3.72 mSv for fixed tube current and 1.57 to 3.35 mSv for AEC scans. In 10-year-old phantom, the ED_{MEAS} values ranged from 1.56 to 2.88 mSv for fixed tube current and 1.63 to 3.14 mSv for AEC scans. In adult phantom, the ED_{MEAS} values ranged from 3.39 to 8.06 mSv for fixed tube current and 2.28 to 3.83 mSv for AEC scans. Mean mAs reduction is linearly related to the ED_{MEAS} reduction ($r^2 = 0.807$, $P < 0.0001$). The absolute percent difference between percent tube current and $\%ED_{MEAS}$ reduction was in most cases higher than 15%.

Conclusions: The reduction in the modulated tube current achieved by AEC should not be used to estimate the reduction in the absorbed dose to exposed radiosensitive organs. Moreover, the reduction in the modulated tube current may only be considered as a rough approximation of the corresponding effective dose reduction.

Key Words: automatic exposure control, effective dose, multidetector CT, organ dose

(*Invest Radiol* 2011;46: 654–662)

Automatic exposure control (AEC) systems constitute the state of the art technique for radiation dose optimization in computed tomography (CT). Modern multidetector-CT scanners allow automatic tube current modulation as the tube rotates around the patient (x-y plane) and/or as the patient travels along the z-axis. A 10% to 53% and a 26% to 43% reduction in radiation dose have been reported for adult[1–6] and pediatric patients,[7] respectively. In these studies dose reduction achieved by AEC was calculated as the percent difference between the preset and the average modulated tube current.

CT examinations constitute partial body exposures. In these exposures, various organs and tissues of the human body may receive substantially different radiation doses. Specific organs and tissues are known to be more radiosensitive than others, and radiation risks are known to differ as a function of age and gender.[8,9] Thus, the dose delivered to each individual radiosensitive organ as well the effect of AEC on the dose absorbed by each organ should be explicitly known for the evaluation of the radiogenic risks. To estimate effective dose in CT imaging, 2 methods have been applied. The first is based on the dose-length product (DLP) and a DLP to effective dose conversion coefficient that depends on the anatomic region being examined. The second is based on the weighted sum of the equivalent doses to different radiosensitive organs of the human body as specified by the International Commission on Radiologic Protection. Several studies have shown that the DLP method provides only a rough estimation of patient effective dose.[10–13] Moreover, according to a recent publication of the International Commission on Radiological Protection (ICRP), the average modulated tube current reduction achieved by AEC activation may not represent the reduction in the dose absorbed by specific organs contained within the body region being scanned.[14] Effective dose (ED), which is calculated as the weighted sum of equivalent doses to different radiosensitive organs of the patient's body,[15] may thus not scale linearly to the average modulated tube current. Although data on organ absorbed dose and ED have been reported for adult standard CT scans performed with fixed tube current, limited data exist on AEC-activated scans. Brisse et al[16] have recently presented results on organ absorbed dose and ED in whole-body CT scans of pediatric anthropomorphic phantoms using a z-axis-based AEC system. However, no data have been presented on the correlation between average modulated tube current and ED. Moreover, several studies have shown that the modern AEC systems, which combine angular

Received December 24, 2010; accepted for publication (after revision) April 19, 2011.

From the *Department of Medical Physics, University Hospital of Heraklion, Crete, Greece; and †Department of Medical Physics, Faculty of Medicine, University of Crete, Crete, Greece.

Conflicts of interest and sources of funding: none declared.

Reprints: Antonios E. Papadakis, PhD, Department of Medical Physics, University Hospital of Heraklion, PO Box 1352, Heraklion 71110, Crete, Greece. E-mail: apapadak@edu.med.uoc.gr.

ISSN: 0020-9996/11/4610-0654

with z-axis tube current modulation, are more efficient in reducing radiation dose compared with z-axis only AEC systems.[17–19] To our knowledge, no data have been published on the effect of such an AEC system on the dose absorbed by each radiosensitive organ and ED in CT imaging.

The purpose of this study was to measure and compare absorbed dose to radiosensitive organs and effective dose associated with standard pediatric and adult CT examinations performed with (a) fixed tube current and (b) AEC-modulated tube current. Additionally, the correlation between the percent reduction of the tube current and of (a) organ doses and (b) effective dose was investigated.

MATERIALS AND METHODS

Phantoms

In all, 4 physical anthropomorphic phantoms (ATOM Phantoms, CIRS, Norfolk, VA) that represent the average individual as neonate, 1-year-old, 5-year-old, 10-year-old child, and the Rando phantom (Alderson Research Labs, Stanford, CA) that simulates the average adult individual were employed (Fig. 1). These phantoms are prepared by radiologically tissue-equivalent material and their internal structure includes artificial skeleton, lung, and soft-tissue, formulated for accurate simulation of human anatomy. Each phantom is subdivided into contiguous 2.5-cm thick sections. Each section contains several holes to allow thermoluminescent dosimeter (TLD) positioning. Weight and height values of the phantoms are listed in Table 1.

CT System and Automatic Exposure Control Mechanism

A 16-slice CT scanner (Sensation 16, Siemens, Germany) was used. This scanner is equipped with a state of the art AEC system (CARE Dose 4D, software version syngo CT 2006G, Siemens, Erlangen, Germany). AEC is accomplished by modulating the tube current both angularly (x-y plane) and along the z-axis of the patient according to each patient's individual anatomy. An image quality reference milliampere-second (mAs_{QR}) value is predefined for every scan protocol. This value corresponds to the effective milliampere-second value that the operator would apply for a "reference patient" during the scan without the use of the AEC. The effective milliampere-second value is defined as the product of the tube current (mA) and the tube rotation time (s) divided by the pitch (p). The pitch is defined as the ratio between the table feed per rotation and x-ray beam width. The reference patient is defined as a typical adult weighing 70 kg to 80 kg (for adult protocols), or as a 5-year-old typical child weighing 20 kg (for pediatric protocols).[20] The modulation strength was set to average decrease–average increase. Being the default, this setting is expected to be followed in the every day clinical practice by most institutions. Detailed information on the operation characteristics of angular and z-axis tube current modulation can be found elsewhere.[21–24]

FIGURE 1. A picture of the anthropomorphic phantoms used in this study. Shown from left to right is the neonate, 1-year-old, 5-year-old, 10-year-old, and the adult phantom.

TABLE 1. Weight and Height Values of Each Phantom

	Age				
	Neonate	**1-y-Old**	**5-y-Old**	**10-y-Old**	**Adult**
Weight (kg)	3.5	10	19	32	73.5
Height (cm)	51	75	110	140	173

Organ Dose Measurements

Lithium fluoride (TLD-100) and calcium fluoride (TLD-200) (Harshaw, OH) chips, 3 × 3 × 0.9 mm, were used to determine the dose imparted to all radiosensitive organs of each phantom according to the ICRP.[15] TLD-100 chips were used for organs located within the primary irradiated volume, whereas TLD-200 chips were used for organs located up to ± 20 cm beyond the limits of the primary irradiated volume. The dose to organs located outside the above range was assumed to be negligible. TLDs-200 are considered preferable compared with TLDs-100 for dose measurement at body sites far from the primarily irradiated volume because they offer 300 times higher sensitivity.[25] All TLDs were calibrated in air against a known dose delivered by a conventional x-ray tube. Dose measurements were performed using the Barracuda x-ray multimeter (RTI Electronics, Mölndal, Sweden). TLD calibration was performed at 80 and 120 kVp. To match the half-value layer of the CT scanner sheets of aluminum of appropriate thicknesses were added at the exit window of the radiologic tube. A Harshaw-3500 reader (ThermoFisher Scientific, Waltham, MA) was used to readout the irradiated TLDs. The calibration coefficient (C) of each TLD was determined as the dose to air ratio recorded by the multimeter divided by the TLD signal. On the basis of their sensitivity, TLDs were grouped into batches so that the standard deviation of each batch was less than 3%. The background signal of each TLD was measured. The minimum detectable radiation dose for each TLD batch was estimated to be 2 SD of the background signal. The minimum detectable radiation dose for TLDs-200 was 10 μGy. Conversion of the TLD signal to absorbed dose was performed by using the following equation:

$$M_x = [(\mu_{en}/\rho)_x/(\mu_{en}/\rho)_{air}] \times (C) \times (TLD_{signal}) \quad (1)$$

where $(\mu_{en}/\rho)_x$ is the mass energy absorption coefficient of the organ at interest and $(\mu_{en}/\rho)_{air}$ the mass energy absorption coefficient of air. Separate mass energy absorption coefficient values at the energies used for the simulated exposures were used for soft-tissue, lung, breast, and bone.[26] Each phantom was loaded with TLDs to measure organ doses for head and neck, thorax, and abdomen and pelvis standard CT scans. The total number of TLDs used for each head and neck acquisition ranged from 90 for neonate to 125 for adult, for each thorax acquisition ranged from 71 for neonate to 195 for adult,

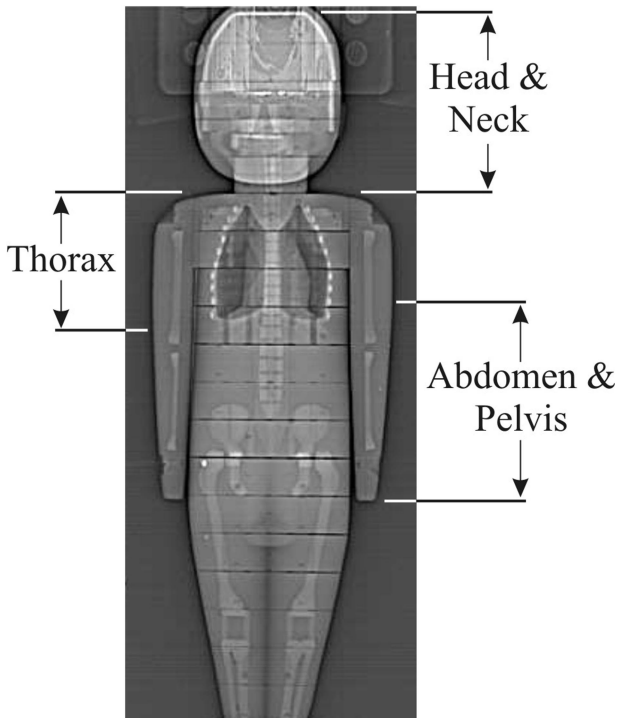

FIGURE 2. The boundaries of the examined anatomic regions shown on an anterior-posterior whole-body topogram of the neonate.

and for each abdomen and pelvis acquisition ranged from 77 for neonate to 223 for adult. Figure 2 illustrates the scan boundaries on an anterior-posterior topogram of the neonate phantom. The scanning parameters were those prescribed by the routine examination protocols of the CT manufacturer (Table 2). Each phantom was first scanned with fixed tube current and then with the AEC activated. Each scan was repeated 10 times to increase TLD signal and reduce the statistical error of the measurement. To relate the position of each TLD to various organs and tissues of the human body, selected patient CT images of the head and neck, thorax, and abdomen and pelvis of a neonate, 1-year-old, 5-year-old, and 10-year-old child, and an adult were retrieved from our patient database. The weight and height of the selected patients matched with the weight and height values of the 5 phantoms. The location of each radiosensitive organ in the adult phantom was verified using previously published data.[25] Each patient's CT image (2.5 cm slice thickness, 2.5 cm reconstruction increment) was matched to the corresponding slice of the phantom. The bone structures of the head and spine were used as landmarks for image matching. The size and position of each organ on each consecutive patient' CT slice was then projected on the corresponding slice of the phantom. The volume fraction (f_i) of each organ that was included in a single slice was identified for those organs which extended beyond the limit of a single slice (ie, brain, salivary glands, lung, esophagus, liver, colon, stomach). Organ absorbed dose (D_{organ}) was then calculated using the following equation:

$$D_{organ} = \sum_{i=1}^{K} f_i \times \left[\frac{1}{\lambda} \sum_{j=1}^{\lambda} M_x^j \right] \quad (2)$$

where M_x is given by Eq. (1), κ is the total number of phantom slices covered by the organ at interest, λ is the total number of TLD chips per phantom slice which are located within the organ at interest, and TLD^j_{signal} is the TLD signal measured by the jth TLD chip. Entrance skin dose was determined from 4 TLD longitudinal arrays placed along the anterior, posterior, and lateral surfaces of each phantom. Total skin dose was then calculated by multiplying mean entrance skin dose with the corresponding primarily irradiated skin surface divided by total average skin surface.[27] Breast dose was calculated as the mean dose recorded by 8 TLDs placed on the anterior surface of each phantom at the level of the left and right breast. The dose to bone surface and red bone marrow tissue fractions of each phantom slice were determined from TLDs placed close to or within bone equivalent phantom tissue. We did not measure the absorbed dose to extrathoracic tissue, lymph nodes, and muscle. Their contribution to effective dose is minor given that the tissue weighting factor for these tissues is relatively small (<1%). The dose absorbed by these organs was thus omitted in the calculation of effective dose. The uncertainty of the measured organ absorbed dose values SD(D_{organ}) was estimated according to the following equation:

$$SD(D_{organ}) = \sqrt{(SD(C))^2 + (SD(TLD_{signal}))^2} \quad (3)$$

where SD(C) is the uncertainty in the calibration factor C, that is, 3%, and SD(TLD_{signal}) is the uncertainty of the TLD measurement. A total of 30 TLDs belonging to the same batch were irradiated to the same amount of dose using the conventional x-ray tube and then were readout. This procedure was repeated 10 times. The SD(TLD_{signal}) was taken as the SD of the measured mean TLD signal. The obtained

TABLE 2. Protocol Examination Parameters of Pediatric and Adult Standard CT Acquisitions

	Pediatric Phantoms			Adult Phantom		
Parameter	**Head and Neck**	**Thorax**	**Abdomen and Pelvis**	**Head and Neck**	**Thorax**	**Abdomen and Pelvis**
Tube potential (kVp)*	120	120	120	120	120	120
Topogram acquisition†	LAT	A-P	A-P	LAT	A-P	A-P
Quality reference tube current (mAs_{QR})	150	30	55	320	100	160
Beam width (mm)	16 × 1.5	16 × 1.5	16 × 1.5	16 × 1.5	16 × 1.5	16 × 1.5
Pitch	0.55	1.1	1.15	0.55	1.15	0.75
Rotation time (s)	0.75	0.5	0.5	1	0.5	0.5
Reconstruction kernel	C30s	B30f	B30f	H31s	B41f	B30f

*Tube potential, mAs_{QR}, and pitch for neonate body scans was 80 kVp, 33, and 0.75, respectively.
†LAT and A-P indicate topograms acquired in the lateral orientation and anterior-posterior orientation, respectively.
CT indicates computed tomography.

D_{organ} values were compared between fixed tube current and AEC-activated scans using the Student *t* test for paired samples. A significant difference was set at a *P* value of less than 0.05. All statistical computations were processed using the MedCalc software package (MedCalc software, Mariakerke, Belgium).

Effective Dose Estimation

To estimate effective dose, 2 different methods were applied. The first was based on the DLP concept. Standard volume computed tomography dose index ($CTDI_{vol}$) measurements were performed at selected beam collimations and kVp settings, using a 10-cm long pencil ionization chamber (MDH Industries, Monrovia, CA) and a body (32 cm diameter) and head (16 cm diameter) CT polymethyl methacrylate (PMMA) phantom. For pediatric scans, the $CTDI_{vol}$ values determined using the 16-cm PMMA phantom were used for both head and body scans. The $CTDI_{vol}$ values determined using the 16-cm and 32-cm PMMA phantoms were used for adult head and body scans, respectively. The $CTDI_{vol}$ value was multiplied by the scan length to derive DLP per anatomic scan. To calculate effective dose (ED_{DLP}), DLP was multiplied by specific normalized effective dose per DLP conversion factors (k)[28] which were recently published based on ICRP publication 103. Different k values were used according to the age and the examined anatomic region of each phantom as shown in Table 3. These k values have been determined using Monte Carlo simulations on the Oak Ridge National Laboratory mathematical phantoms that mimic newborns, 1-, 5-, and 10-year-old children and adults.[29] Percent ED_{DLP} difference ($\%ED_{DLP}$) achieved by AEC activation was calculated using the following equation:

$$\%ED_{DLP} = \frac{ED_{DLP}^{fixmA} - ED_{DLP}^{AEC}}{ED_{DLP}^{fixmA}} \times 100,$$

where ED_{DLP}^{fixmA} and ED_{DLP}^{AEC} are the ED_{DLP} effective dose values estimated for fixed mA and AEC-activated scans, respectively. The percent difference in ED_{DLP} defined above equal the corresponding percent difference between the fixed mAs_{QR} value and the mean modulated mAs_{AEC} value, which is applied during the AEC-activated scan.

The second method was based on the measurement of the absorbed dose at all radiosensitive organs of each phantom using TLDs. Effective dose (ED_{MEAS}) was estimated as the weighted sum of the measured organ doses according to 2007 recommendations of the ICRP.[15] Percent ED_{MEAS} difference ($\%ED_{MEAS}$) achieved by AEC activation was calculated using the following equation:

$$\%ED_{MEAS} = \frac{ED_{MEAS}^{fixmA} - ED_{MEAS}^{AEC}}{ED_{MEAS}^{fixmA}} \times 100,$$

where ED_{MEAS}^{fixmA} and ED_{MEAS}^{AEC} are the ED_{MEAS} effective dose values estimated for fixed mA and AEC-activated scans, respectively.

TABLE 3. The Effective Dose Per Dose Length Product Conversion Factors Used in This Study for Each Phantom and Anatomical Region According to ICRP Publication 103[23]

	k ($mSvmGy^{-1}cm^{-1}$)				
	Neonate	**1-y-Old**	**5-y-Old**	**10-y-Old**	**Adult**
Head and Neck*	0.0120	0.0085	0.0061	0.0049	0.0032
Thorax	0.0823	0.0467	0.0314	0.0234	0.0145
Abdomen and Pelvis†	0.0855	0.0472	0.0321	0.0231	0.0141

*Conversion factors for the head and neck anatomical region were calculated as the weighted average of the original values tabulated in Table 5 of reference 23 for head and neck, according to the irradiated lengths of the head and the neck regions for each phantom.

†Conversion factors for abdomen and pelvis anatomical region were calculated as the weighted average of the original values tabulated in Table 5 of reference 23 for abdomen and pelvis, according to the irradiated lengths of the abdomen and pelvis regions for each phantom.

ICRP, International Commission on Radiological Protection.

Image Quality Assessment

To assess the effect of AEC on image quality, we have compared the noise in the images obtained from scans performed with fixed mAs_{QR} to the corresponding noise in the images obtained from AEC-activated scans. Image noise was measured as the SD of the mean Hounsfield unit value in circular regions of interest (ROI, 1 cm^2). These ROIs were drawn over uniform soft-tissue equivalent image areas. Five ROIs were drawn in each image slice throughout body regions scanned with fixed mAs_{QR}. These ROIs were copied at exactly the same anatomic locations in the corresponding images obtained from the AEC-activated scans. Quantitative image analysis was performed using the ImageJ image analysis software (version 1.42q, Java, NIH, Bethesda, MD). Image noise measurements were compared for each phantom and anatomic region with regard to scans performed with fixed mAs_{QR} and with the AEC activated. The Student *t* test was used for paired samples. A significant difference was set at a *P* value of less than 0.05.

RESULTS

The measured organ absorbed doses and the effective dose values calculated using the (a) DLP (ED_{DLP}) and (b) organ absorbed doses (ED_{MEAS}) are summarized in Tables 4, 5, and 6. A large variation on the percent dose difference between fixed tube current and AEC-activated scans was found among different organs located within the primary irradiated volume of each phantom. The uncertainty of the measured organ absorbed dose $SD(D_{organ})$ values, listed in Table 4 through 6, were found to be within ± 9.1%.

In head and neck scans, the estimated ED_{DLP} value for each phantom was higher than the corresponding ED_{MEAS} value (Table 4). In thorax and abdomen and pelvis scans, the estimated ED_{DLP} value was higher than ED_{MEAS} value for pediatric phantoms and lower than ED_{MEAS} for the adult phantom (Tables 5, 6). A comparative evaluation of the $\%ED_{MEAS}$ reduction versus the corresponding $\%ED_{DLP}$ reduction achieved by AEC activation in each anatomic region of the phantoms is shown in Table 7. The absolute percent difference between $\%ED_{MEAS}$ and $\%ED_{DLP}$ reduction was found to range from 2.6% to 200%. Figure 3 illustrates the relation between the 2 quantities which can be represented as: $\%ED_{MEAS} = (0.85 \cdot \%ED_{DLP}) + 5.20$. This equation is based on linear regression analysis which shows a significant linear correlation between $\%ED_{MEAS}$ and $\%ED_{DLP}$ ($r^2 = 0.807$, $P < 0.0001$).

Table 8 lists the image noise values measured in the images obtained with fixed mAs_{QR} scans compared with the noise values obtained with AEC-activated scans. A statistically significant change in the image noise is recorded in many AEC-activated scans ($P < 0.05$). Moreover, Table 8 illustrates that image noise increases in anatomic scans where mAs_{AEC} decreases, whereas image noise decreases in anatomic scans where mAs_{AEC} increases.

DISCUSSION

The latest advances in CT technology have led to a significant increase in the frequency of CT examinations. Patient radiation dose resulting from CT examinations is an issue of great concern given that CT is considered a high-radiation dose imaging modality.[30–34] In this study, the effect of AEC on organ and effective dose in

TABLE 4. Organ Doses (mGy), $CTDI_{vol}$ (mGy), Scan Length (cm), and Effective Doses (mSv) for Fixed Tube Current (mA) and AEC-Activated Head and Neck CT Scans of Each Phantom

	Doses for Fixed Tube Current and AEC-Activated Head and Neck CT Scans									
	Neonate		1-y-Old		5-y-Old		10-y-Old		Adult	
Organ/Tissue	Fixed mA/AEC	% Difference	Fixed mA/AEC	% Difference	Fixed mA/AEC	% Difference	Fixed mA/AEC	% Difference	Fixed mA/AEC	% Difference
Bone marrow	8.33/5.00	39.9	3.80/2.64	30.5	6.12/4.74	22.5	3.51/3.02	14.0	4.71/3.94	16.3
Thyroid	25.19/14.61	42.0	8.49/3.07	63.8	11.8/9.39	20.4	28.4915.68	44.9	30.37/18.11	40.3
Bone surface	12.05/7.39	38.6	5.92/4.12	30.4	9.52/7.37	22.5	5.46/4.7	13.9	8.57/6.11	28.7
Skin	4.50/3.30	26.6	3.93/3.61	8.1	2.68/2.76	−2.9*	2.28/2.48	−8.7	7.57/3.77	50.1
Brain	14.74/9.14	37.9	17.34/14.17	18.2	15.18/12.50	17.6	18.17/15.17	16.5	29.72/23.82	19.8
Salivary glands	22.53/14.22	36.8	10.64/7.29	31.4	19.73/15.45	21.6	19.57/14.99	23.4	51.71/32.06	38.0
$CTDI_{vol}$ (mGy)	30.33/19.98	34.1	30.33/23.62	22.1	30.33/23.20	23.5	30.33/17.80	41.3	64.76/42.80	33.9
Scan length (cm)	11.8		17.2		17.1		21.9		21.6	
ED_{DLP} (mSv)	4.30/2.83	34.1	4.42/3.44	22.1	3.15/2.41	23.5	3.24/1.90	41.3	4.48/2.96	33.9
ED_{MEAS} (mSv)	3.23/1.73	46.4	1.71/0.99	42.1	2.03/1.57	22.6	2.75/1.78	35.1	3.39/2.28	32.7

Dose values are listed only for the main radiosensitive organs located within the primary irradiated volume.
*Nonsignificant difference between fixed and AEC-activated scan.
$CTDI_{vol}$ indicates standard volume computed tomography dose index; AEC, automatic exposure control; CT, computed tomography.

TABLE 5. Organ Doses (mGy), $CTDI_{vol}$ (mGy), Scan Length (cm), and Effective Doses (mSv) for Fixed Tube Current (mA) and AEC-Activated Thorax CT Scans of Each Phantom

	Organ Doses (mGy) and Effective Doses (mSv) for Fixed Tube Current and AEC-Activated Thorax CT Scans									
	Neonate		1-y-Old		5-y-Old		10-y-Old		Adult	
Organ/Tissue	Fixed mA/AEC	% Difference	Fixed mA/AEC	% Difference	Fixed mA/AEC	% Difference	Fixed mA/AEC	% Difference	Fixed mA/AEC	% Difference
Lung	1.92/2.42	−26.1	3.74/2.92	21.9	3.83/3.37	12.0	3.34/3.07	8.0	9.04/6.40	29.2
Stomach	1.55/1.52	1.5*	0.39/0.40	−2.5*	1.94/2.9	−7.7	1.44/1.82	−26.3	5.89/5.56	5.6
Bone marrow	0.79/0.84	−6.3	0.92/0.76	17.3	0.97/0.93	4.1	0.86/0.78	9.3	2.93/2.01	31.3
Breast	1.89/2.29	−21.3	3.50/2.86	18.2	3.39/2.87	15.3	3.20/3.35	−4.6	4.52/3.08	31.8
Thyroid	3.17/3.00	5.2	2.09/1.30	37.7	9.02/10.9	−20.8	0.71/1.15	−61.9	3.88/2.24	42.2
Oesophagus	1.79/1.76	1.3*	3.29/2.92	11.2	3.45/3.06	11.3	3.09/2.86	7.4	8.53/5.71	33.0
Liver	1.61/1.76	−9.5	2.28/1.76	22.8	1.68/1.65	1.7*	0.83/0.89	−7.2	4.02/3.24	19.4
Bone surface	1.03/0.93	9.9	1.43/1.18	17.4	1.44/1.37	4.8	1.34/1.22	8.9	3.20/1.93	39.6
Skin	0.27/0.31	−16.8	0.55/0.45	18.9	0.53/0.45	15.4	0.50/0.52	−4.4	0.74/0.50	31.8
$CTDI_{vol}$ (mGy)	2.42/2.83	−17.1	6.06/5.44	10.1	6.06/5.66	6.6	6.06/6.68	−10.3	7.26/6.16	15.1
Scan length (cm)	9.4		15		19.2		23.5		29.2	
ED_{DLP} (mSv)	1.87/2.19	−17.1	4.23/3.80	10.1	3.64/3.40	6.6	3.33/3.67	−10.3	3.07/2.60	15.1
ED_{MEAS} (mSv)	1.18/1.31	−10.5	1.85/1.47	20.4	2.20/2.15	2.2	1.56/1.63	−4.0	3.94/2.94	25.4

Dose values are listed only for the main radiosensitive organs located within the primary irradiated volume.
*Nonsignificant difference between fixed and AEC activated scan.

pediatric and adult standard CT examinations was investigated. Our results revealed that (i) percent dose reduction varies considerably among different radiosensitive organs located within the anatomic region being scanned and (ii) percent effective dose reduction deviates considerably from the corresponding reduction in the average modulated tube current.

Several studies have been conducted on the efficacy of AEC systems for dose reduction.[1–7,17–19,21–24,35–37] These studies have reported results on the percent dose reduction based on the average reduction of the modulated tube current applied within the examined anatomic region. Recently, Brisse et al[16] have investigated the effect of a z-axis-based AEC system on organ absorbed dose and effective dose associated with whole-body pediatric CT imaging. Several studies have shown that the AEC systems, which combine angular with z-axis tube current modulation, are more efficient in reducing radiation dose. To our knowledge, this is the first study aimed to provide a detailed insight to the effect of such an AEC system on the dose delivered to each individual radiosensitive organ in pediatric and adult standard CT examinations. Our results demonstrate that the percent dose reduction provoked by the AEC system varies considerably among primarily exposed organs (Tables 4, 5, 6). Moreover, AEC may considerably increase the organ absorbed dose in pediatric phantoms. The magnitude of these variations may be related to the anatomic location of each organ as well as patient's size.[38,39] The radiation intensity is kept constant throughout a helical scan when performed with fixed tube current. In AEC-activated

TABLE 6. Organ Doses (mGy), $CTDI_{vol}$ (mGy), Scan Length (cm), and Effective Doses (mSv) for Fixed Tube Current (mA) and AEC-Activated Abdomen and Pelvis CT Scans of Each Phantom

	Organ Doses (mGy) and Effective Doses (mSv) for Fixed Tube Current and AEC-Activated Abdomen and Pelvis CT Scans									
	Neonate		1-y-Old		5-y-Old		10-y-Old		Adult	
Organ/Tissue	Fixed mA/AEC	% Difference	Fixed mA/AEC	% Difference	Fixed mA/AEC	% Difference	Fixed mA/AEC	% Difference	Fixed mA/AEC	% Difference
Lung	0.48/0.53	−12.1	0.36/0.25	30.5	1.28/1.36	−6.2	0.06/0.071	−18.3	2.19/0.98	55.2
Stomach	2.41/1.94	19.3	6.40/4.72	26.2	6.68/6.44	3.5*	2.52/3.15	−25.0	14.42/6.61	54.1
Colon	1.66/1.79	−8.1	6.11/6.41	−4.9	6.88/6.27	8.8	5.91/7.21	−21.9	17.47/8.22	52.9
Bone marrow	0.13/0.10	22.3	1.36/1.08	20.5	2.04/1.68	17.6	1.82/2.14	−17.5	4.15/2.05	50.6
Gonads	2.27/1.62	28.3	0.71/0.53	25.3	5.99/4.41	26.3	4.97/6.24	−25.5	13.35/7.93	40.5
Oesophagus	1.27/0.90	29.1	0.30/0.22	26.6	1.36/1.52	−11.7			1.72/0.48	72.0
Bladder	1.70/1.44	15.2	5.99/5.36	10.5	6.59/4.02	38.9	4.71/7.65	−62.4	12.99/7.13	45.1
Liver	1.50/1.11	25.6	4.57/3.43	24.9	6.55/6.61	−0.9*	3.86/4.82	−24.8	13.53/5.84	56.8
Bone surface	1.80/1.50	16.3	2.12/1.69	20.2	3.17/2.62	17.3	2.83/3.32	−17.3	2.46/1.19	51.6
Skin	0.56/0.42	24.3	1.64/1.23	24.6	1.34/1.19	10.8	1.18/1.52	−29.0	2.71/1.87	31.0
$CTDI_{vol}$ (mGy)	2.42/2.02	16.5	11.11/9.11	18.0	11.11/8.47	23.7	11.11/13.50	−21.6	11.61/5.36	53.8
Scan length (cm)	14.7		14.9		29.2		33.0		42.9	
ED_{DLP} (mSv)	3.03/2.53	16.5	7.80/6.39	18.0	10.41/7.94	23.7	8.45/10.28	−21.6	7.02/3.24	53.8
ED_{MEAS} (mSv)	1.29/1.17	9.3	2.82/2.38	15.6	3.72/3.35	9.9	2.88/3.14	−8.9	8.06/3.83	52.4

Dose values are listed only for the main radiosensitive organs located within the primary irradiated volume.
*Non significant difference between fixed and AEC-activated scan.

TABLE 7. A Comparative Evaluation of the $\%ED_{MEAS}$ Versus $\%ED_{DLP}$ Achieved in AEC-Activated Scans

	$\%ED_{MEAS}$	$\%ED_{DLP}$	% Difference $\left[\frac{\lvert \%ED_{MEAS} - \%ED_{DLP} \rvert}{\%ED_{MEAS}} \times 100\right]$
Head and neck			
Neonate	46.4	34.1	26.5
1-yr-old	42.1	22.1	47.5
5-yr-old	22.6	23.5	3.9
10-yr-old	35.1	41.3	17.6
Adult	32.7	33.9	3.6
Thorax			
Neonate	−10.5	−17.1	62.8
1-yr-old	20.4	10.1	50.5
5-yr-old	2.2	6.6	200
10-yr-old	−4.0	−10.3	157.5
Adult	25.4	15.1	40.5
Abdomen and pelvis			
Neonate	9.30	16.5	77.4
1-yr-old	15.6	18.0	15.3
5-yr-old	9.9	23.7	139.3
10-yr-old	−8.9	−21.6	142.6
Adult	52.4	53.8	2.6

The absolute percent difference between $\%ED_{MEAS}$ and $\%ED_{DLP}$ is also shown.
*$\%ED_{DLP}$ difference values achieved with AEC activation equal the corresponding %mA difference values.

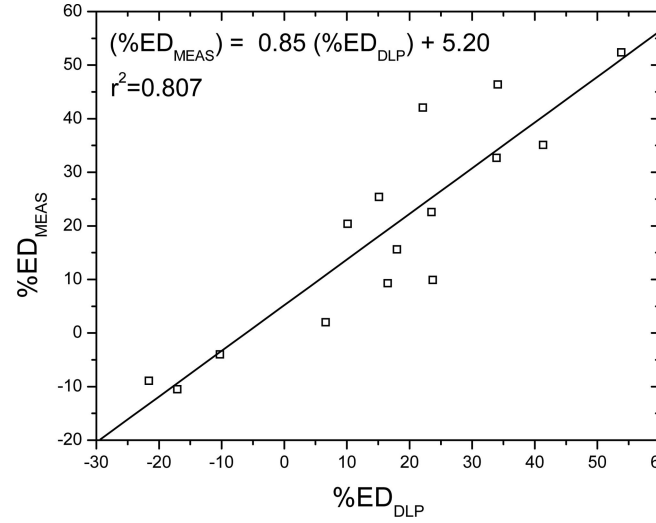

FIGURE 3. The correlation between $\%ED_{MEAS}$ and $\%ED_{DLP}$ values derived from head and neck, thorax, and abdomen and pelvis AEC-activated CT scans of the 5 anthropomorphic phantoms.

scans the radiation intensity is on line varied both angularly, according to the patient's attenuation profile in the x-y plane, and along z-axis based on the attenuation data retrieved from the topogram acquisition. For organs located in lateral positions with a high difference between anterior-posterior and lateral attenuation, the percent dose reduction due to AEC activation is expected to be lower compared with organs located in positions with less anterior-posterior to lateral attenuation difference. For instance, in abdomen and pelvis scans of the adult phantom the percent dose difference is 56.8% for liver compared with 72.0% for esophagus. Moreover, for organs located in positions with relatively high attenuation, the percent dose reduction is expected to be lower compared with organs which are located at less attenuating positions. For example, percent dose reduction is 40.5% for gonads compared with 55.2% for lung and 72.0% for esophagus in the abdomen and pelvis scan of

TABLE 8. Mean Image Noise (SD) Values Measured in Images Obtained From Scans Performed With (a) Fixed mAs_{QR} and (b) AEC

	Image Noise		
	Head and Neck	Thorax	Abdomen and Pelvis
Neonate			
Fixed mAs_{QR}	4.4 ± 2.5	10.8 ± 1.2	10.4 ± 2.0
AEC	4.3 ± 2.6*	9.0 ± 1.6	12.0 ± 0.9*
1			
Fixed mAs_{QR}	3.4 ± 0.8	7.2 ± 1.0	8.5 ± 1.3
AEC	3.9 ± 0.6	7.0 ± 1.5*	7.9 ± 1.5*
5			
Fixed mAs_{QR}	3.4 ± 1.1	7.9 ± 2.0	10.1 ± 0.9
AEC	4.1 ± 1.2	8.0 ± 1.4*	7.1 ± 0.7
10			
Fixed mAs_{QR}	2.9 ± 0.5	8.2 ± 1.5	9.0 ± 1.7
AEC	3.6 ± 0.5	7.7 ± 0.6*	8.8 ± 1.5*
Adult			
Fixed mAs_{QR}	3.3 ± 1.4	9.9 ± 1.0	9.5 ± 1.1
AEC	3.9 ± 0.7	10.5 ± 1.7*	13.9 ± 1.1

*Nonsignificant difference between fixed mAs_{QR} and AEC-activated scan.

the adult phantom. The variation in the recorded percent dose reduction may be also attributed to the anatomy of the tissues surrounding the organ at interest. For instance, gonads are surrounded by more bone (ie, pelvis) than esophagus. This may affect the magnitude of tube current modulation and thus the percent dose reduction for such organs. Another reason that might explain the variance in the recorded percent dose difference provoked by the AEC activation among organs is that the tube angle at the start of each scan might not be the same between fixed mA and AEC-activated scans. To directly compare the dose delivered to a specific organ during a fixed mA to the corresponding dose delivered from an AEC-activated scan, the beam angular locations irradiating the organ at interest should coincide between the 2 scans. Given that clinically, CT scanners do not allow the control of the tube start angle, it is reasonable to assume that the position of the tube was different between the scans. However, the effect of the random position of the irradiation beam on the percent organ dose reduction is considerably minimized if each fixed mA and AEC-activated scan is repeated 10 times.

Our results on percent organ dose reduction deviate considerably from the percentED_{MEAS} reduction. Typically, in thorax scans of the 5-year-old phantom, a 12.0% and 15.3% dose decrease for lung and breast, respectively and a 20.8% dose increase for thyroid are associated with a 2.2% reduction in ED_{MEAS} (Table 5). In abdomen and pelvis scans of the 10-year-old phantom, a 25.0% and 62.4% dose increase for stomach and bladder, respectively was associated with an 8.9%ED_{MEAS} increase (Table 6). The percentage of absolute difference between percent tube current and %ED_{MEAS} reduction was higher than 15% in all scans with the exception of head and neck scan of the 5-year-old phantom and the head and neck and abdomen and pelvis scans of the adult phantom (Table 7). These findings suggest that in AEC-activated scans percent reduction in the tube current represents only a rough estimate of dose reduction. This value should not be considered equal to effective dose reduction. Furthermore, percent tube current reduction should not be used as an estimate of organ dose reduction. The equation derived from the linear regression analysis between %ED_{MEAS} and %ED_{DLP} can be used to describe the relation between the 2 quantities for a specific AEC-activated CT examination. To estimate %ED_{MEAS} reduction the user may substitute the %ED_{DLP} quantity in the equation shown in Figure 3 with the percent reduction of the average modulated tube current.

To assess the effect of AEC on the radiation dose delivered by each scan, we have calculated the percent difference between the dose values obtained from scans performed with the default reference mAs_{QR} and mean modulated mAs_{AEC}. As described in section (CT System and Automatic Exposure Control Mechanism), the default reference mAs_{QR} in a pediatric protocol corresponds to the value that the user would choose for a 5-year-old typical child. In this study, we have applied the same mAs_{QR} values for all pediatric phantoms based on the guidelines given by the operator's manual,[20] that is, 150 for head and neck, 30 for thorax, and 55 for abdomen and pelvis scans (Table 2). Alternatively, AEC-activated scans could be compared with the corresponding fixed tube current scans by taking into account the manually adapted tube current according to the weight of each phantom. As observed in Tables 5 and 6, AEC induces an increase in effective dose values for thorax and abdomen and pelvis scans of the 10-year-old phantom. This increase is in turn associated with an image noise decrease (Table 8). It is apparent that AEC should increase the tube current for a 10-year-old child for which the default reference mAs_{QR} value is intended. The 10-year-old phantom exhibits higher x-ray attenuation compared with the 5-year-old phantom, therefore higher radiation dose is needed to maintain diagnostic image quality.

To calculate ED_{DLP}, we have used the new DLP to ED conversion factors that were recently presented by Deak et al.[28] These factors were derived using the latest ICRP 103 recommendations and were found to be significantly higher than the corresponding values determined using the ICRP 60 recommendations.[40] To our knowledge, this is the first study that employs ICRP 103-based conversion factors to calculate ED_{DLP} in pediatric and adult CT imaging. The ED_{DLP} values, calculated using the DLP method, differ considerably from the corresponding ED_{MEAS} measured values. In head and neck scans, ED_{DLP} overestimates effective dose for all phantoms (Table 4). In thorax and abdomen and pelvis scans, ED_{DLP} overestimates effective dose for all pediatric phantoms (Table 5, 6). To calculate ED_{DLP} for pediatric body scans, we have used the $CTDI_{vol}$ values measured using the 16-cm PMMA phantom. These values are higher than the corresponding values measured on the 32-cm phantom. The use of $CTDI_{vol}$ values measured on cylindrical PMMA phantoms of variable diameter, which would more closely approach the body size of a child at various ages, would be more appropriate. In reference to the adult phantom, effective dose is underestimated by the DLP method by 22.0% in thorax and 12.9% in abdomen and pelvis in fixed tube current scans. These results are in agreement with Hurwitz et al[41,42] who have reported that the underestimation of ED using ED_{DLP} in fixed tube current protocols is 23.6% for coronary CT angiography scans, 18% for standard abdomen and pelvis scans,[41] and 36.1% for pulmonary vein scans.[42] Thomas and Wang[43] have recently reported results on the estimation of ED_{DLP} in pediatric patients undergoing fixed mA standard CT examinations. The ED_{DLP} values presented were considerably higher than those derived in this study. For thorax scans, the ED_{DLP} was reported to range from 2.8 versus 1.87 mSv for neonates to 4.1 versus 2.23 mSv for 10-year-old children. The corresponding ED_{DLP} values for abdomen and pelvis scans ranged from 13.1 versus 3.03 mSv for neonates to 8.9 versus 8.45 mSv for 10-year-old children. These differences are mainly attributed to the different scanning parameters applied during CT acquisition. A 120 kVp tube potential was used in neonate torso scans versus 80 kVp in this study. Moreover, significantly higher mAs values were used by

Thomas and Wang[43] which ranged from 42 to 96 versus 30 for thorax scans and 60 to 120 versus 55 for abdomen and pelvis scans.

Effective dose is a quantity that reflects the radiation detriment of a nonuniform exposure in terms of an equivalent whole-body exposure. To estimate this quantity, we have used the tissue weighting factors provided by ICRP.[15] These factors have been derived from epidemiological studies of cancer induction as well as from experimental genetic data of human beings averaged over all ages and both the sexes, after radiation exposure. The anthropomorphic adult phantom used in our study represents a reference person and it is thus well suited for effective dose estimation. Besides, the anthropomorphic pediatric phantoms employed in this study represent the average individual as neonate, 1-year-old, 5-year-old, and 10-year-old child. There is absence of appropriate weighting factors describing the radiosensitivity of each organ in pediatric subjects. To estimate effective dose for these subjects, we have used the weighing factors described earlier for the reference adult person. We recognized that this method may underestimate ED, given that the radiosensitivity of pediatric organs and tissues is higher compared with adults. These tissue weighting factors have been used for the estimation of effective dose in pediatric x-ray imaging by various investigators.[44–46]

For partial body exposures, when various organs and tissues receive substantially different radiation doses, the assessment and interpretation of effective dose may be problematic.[15] Different organs exhibit variable sensitivity to ionizing radiation, and the radiogenic risks depend on patient's sex and age at exposure. Thus, for the evaluation of radiogenic risk, absorbed doses to organs and tissues should be used instead of effective dose.[14,15] In this study, we have measured the absorbed dose delivered to each radiosensitive organ by standard partial body CT exposures of reference pediatric and adult subjects. Moreover, we have assessed the effect of AEC activation on the organ absorbed doses. These data can be used to evaluate the associated radiogenic risk separately for each organ and phantom as well as the effect of AEC on the radiogenic risk. The risk for radiation-induced fatal cancer may be determined by multiplying organ absorbed dose with appropriate nominal risk coefficients. These coefficients have been determined on the basis of risk estimates specific to various cancer sites in large cohort epidemiological studies.[15,47]

A limitation of this study is that extrathoracic tissue, lymph nodes, and muscle absorbed doses were not included in the weighted sum for the calculation of the effective dose. The exact location and distribution of these organs/tissues is difficult to be delineated within the phantoms. However, the contribution of their weighted absorbed doses to effective dose is expected to be negligible. Another limitation of our study is that the use of tissue weighting factors provided by ICRP[15] for the adult reference person may underestimate effective dose in children, given that the radiosensitivity of pediatric organs and tissues is higher compared with adults. These considerations may affect the absolute values of effective dose for pediatric phantoms. However, they do not alter our results on the percent tube current and $\%ED_{MEAS}$ reduction. It should be noted that our results provide an estimate of the reduction in the percent organ dose and effective dose owing to AEC activation for standard CT examinations performed in anthropomorphic phantoms. The actual dosimetric data for any individual may vary from patient to patient depending on the patient size, z coverage, and scanning parameters.

CONCLUSION

This study showed that percent dose reduction achieved by AEC varies considerably among different organs located within the primary irradiated scan volume. In adult CT scans, AEC activation implied a reduction in radiation exposure. However, in pediatric scans a potential increase in organ absorbed dose may be invoked. The percent difference between percent tube current reduction and effective dose reduction was predominantly higher than 15%. Therefore, in AEC-activated CT scans the percent reduction in the modulated tube current does not represent an accurate estimate of percent effective dose reduction. Moreover, percent reduction in the modulated tube current should not be used to estimate the reduction in absorbed dose to individual radiosensitive organs.

REFERENCES

1. Greess H, Wolf H, Baum U, et al. Dose reduction in computed tomography by attenuation-based on-line modulation of tube current: evaluation of six anatomical regions. *Eur Radiol*. 2000;10:391–394.
2. Hundt W, Rust F, Stabler A, et al. Dose reduction in multislice computed tomography. *J Comput Assist Tomogr*. 2005;29:140–147.
3. Tack D, De Maertelaer V, Gevenois PA. Dose reduction in multidetector CT using attenuation-based online tube current modulation. *Am J Roentgenol*. 2003;181:331–334.
4. Das M, Mahnken AH, Muhlenbruch G, et al. Individually adapted examination protocols for reduction of radiation exposure for 16-MDCT chest examinations. *Am J Roentgenol*. 2005;184:1437–1443.
5. Greess H, Wolf H, Baum U, et al. Dosage reduction in computed tomography by anatomy-oriented attenuation-based tube-current modulation: the first clinical results. *Rofo*. 1999;170:246–250.
6. Gies M, Kalender WA, Wolf H, et al. Dose reduction in CT by anatomically adapted tube current modulation. I: simulation studies. *Med Phys*. 1999;26:2235–2247.
7. Greess H, Lutze J, Nomayr A, et al. Dose reduction in subsecond multislice spiral CT examination of children by on-line tube current modulation. *Eur Radiol*. 2004;14:995–999.
8. Food and Drug Administration (FDA) Public health notification:reducing radiation risk from computed tomography for pediatric and small adult patients. *Pediatr Radiol*. 2002;32:314–316.
9. Brody AS, Frush DP, Huda W, et al. Radiation risk to children from computed tomography. *Pediatrics*. 2007;120:677–682.
10. Christner JA, Kofler JM, McCollough CH. Estimating effective dose for CT using dose-length product compared with using organ doses: consequences of adopting International Commission on Radiological Protection Publication 103 or dual-energy scanning. *Am J Roentgenol*. 2010;194:881–889.
11. Dietze G, Harrison JD, Menzel HG. Effective dose: a flawed concept that could and should be replaced. *Br J Radiol*. 2009;82:348–350.
12. Brenner DJ, McCollough CH, Orton CG. It is time to retire the computed tomography dose index (CTDI) for quality assurance and dose optimization. *Med Phys*. 2006;33:1189–1191.
13. Perisinakis K, Damilakis J, Tzedakis A, et al. Determination of the weighted CT dose index in modern multi-detector CT scanners. *Phys Med Biol*. 2007;52:6485–6495.
14. International Commission on Radiological Protection. Managing patient dose in multi-detector computed tomography (MDCT). ICRP publication 102. *Ann ICRP*. 2007:1–79.
15. International Commission on Radiological Protection. The 2007 recommendations of the International Commission on Radiological Protection. ICRP publication 103. *Ann ICRP*. 2007:1–332.
16. Brisse H, Robilliard M, Savignoni A, et al. Assessment of organ absorbed doses and estimation of effective doses from pediatric anthropomorphic phantom measurements for multi-detector row CT with and without automatic exposure control. *Health Phys*. 2009;97:303–314.
17. Papadakis AE, Perisinakis K, Damilakis J. Automatic exposure control in pediatric and adult multi-detector CT examinations: a phantom study on dose reduction and image quality. *Med Phys*. 2008;35:4567–4576.
18. Mulkens TH, Bellinck P, Baeyaert M, et al. Use of an automatic exposure control mechanism for dose optimization in multi-detector row CT examinations: clinical evaluation. *Radiology*. 2005;237:213–223.
19. Rizzo S, Kalra M, Schmidt B, et al. Comparison of angular and combined automatic tube current modulation techniques with constant tube current CT of the abdomen and pelvis. *Am. J. Roentgenol*. 2006;186:673–679.
20. Bredenholler C, Feuerlein U. Somatom sensation 16. Application guide. Erlangen, Germany: Siemens Medical; 2006.
21. Kalra M, Maher M, Kamath R, et al. Sixteen-detector row CT of abdomen and pelvis: study for optimization of z-axis modulation technique performed in 153 patients. *Radiology*. 2004;233:241–249.

22. Kalra M, Maher M, Toth T, et al. Techniques and applications of automatic tube current modulation for CT. *Radiology*. 2004;233:649–657.
23. Kalender WA, Wolf H, Suess C. Dose reduction in CT by anatomically adapted tube current modulation. II: phantom measurements. *Med Phys*. 1999;26:2248–2253.
24. McCollough C, Bruesewitz M, Kofler JM. CT dose reduction and dose management tools: overview of available options. *Radiographics*. 2006;26: 503–512.
25. Perisinakis K, Theocharopoulos N, Karkavitsas N, et al. Patient effective radiation dose and associated risk from transmission scans using ^{153}Gd line sources in cardiac SPECT studies. *Health Phys*. 2002;83:66–74.
26. Hubbell JH, Seltzer SM. Tables of x-ray mass attenuation coefficients and mass energy-absorption coefficients from 1 keV to 20 MeV for elements Z = 1 to 92 and 48 additional substances of dosimetric Interest. The National Institute of Standards and Technology (NIST). Available at: http://www.nist.gov. Accessed November 25, 2010.
27. International Commission on Radiological Protection. Report of the task group on reference man. ICRP publication 23; 1992.
28. Deak PD, Smal Y, Kalender WA. Multisection CT protocols: sex- and age-specific conversion factors used to determine effective dose from dose-length product. *Radiology*. 2010;257:158–166.
29. Cristy M. Mathematical phantoms representing children of various ages for use in estimates of internal dose. Report number ONRL/NUREG/TM-367. OAK Ridge, Tenn: Oak Ridge National Laboratory; 1980.
30. Brix G, Lechel U, Petersheim M, et al. Dynamic contrast-enhanced CT studies: balancing patient exposure and image noise. *Invest Radiol*. 2011;46: 64–70.
31. Lell MM, May M, Deak P, et al. High-pitch spiral computed tomography: effect on image quality and radiation dose in pediatric chest computed tomography. *Invest Radiol*. 2011;46:116–123.
32. Schenzle JC, Sommer WH, Neumaier K, et al. Dual energy CT of the chest: how about the dose? *Invest Radiol*. 2010;45:347–353.
33. Prakash P, Kalra MK, Kambadakone AK, et al. Reducing abdominal CT radiation dose with adaptive statistical iterative reconstruction technique. *Invest Radiol*. 2010;45:202–210.
34. Kuefner MA, Hinkmann FM, Alibek S, et al. Reduction of x-ray induced DNA double-strand breaks in blood lymphocytes during coronary CT angiography using high-pitch spiral data acquisition with prospective ECG-triggering. *Invest Radiol*. 2010;45:182–187.
35. Papadakis AE, Perisinakis K, Damilakis J. Angular on-line tube current modulation in multidetector CT examinations of children and adults: the influence of different scanning parameters on dose reduction. *Med Phys*. 2007;34:2864–2874.
36. Kalra M, Maher M, Toth T, et al. Comparison of z-axis automatic tube current modulation technique with fixed tube current CT scanning of abdomen and pelvis. *Radiology*. 2004;232:347–353.
37. van Straten M, Deak P, Shrimpton PC, et al. The effect of angular and longitudinal tube current modulations on the estimation of organ and effective doses in x-ray computed tomography. *Med Phys*. 2009;36:4881–4889.
38. Zhang D, Savandi AS, Demarco JJ, et al. Variability of surface and center position radiation dose in MDCT: Monte Carlo simulations using CTDI and anthropomorphic phantoms. *Med Phys*. 2009;36:1025–1038.
39. Di Zhang, Zankl M, DeMarco JJ, et al. Reducing radiation dose to selected organs by selecting the tube start angle in MDCT helical scans: a Monte Carlo based study. *Med Phys*. 2009;36:5654–5664.
40. American Association of Physicists in Medicine. The measurement, reporting, and management of radiation dose in CT. New York, NY: AAPM; 2008:1–28. Report number 96.
41. Hurwitz L, Yoshizumi T, Goodman P, et al. Effective dose determination using an anthropomorphic phantom and metal oxide semiconductor field effect transistor technology for clinical adult body multidetector array computed tomography protocols. *J Comput Assist Tomogr*. 2007;31:544–549.
42. Hurwitz L, Reiman RE, Yoshizumi TT, et al. Radiation dose from contemporary cardiothoracic multidetector CT protocols with an anthropomorphic female phantom: implications for cancer induction radiology. 2007;245:742–750.
43. Thomas KE, Wang B. Age-specific effective doses for pediatric MSCT examinations at a large children's hospital using DLP conversion coefficients: a simple estimation method. *Pediatr Radiol*. 2008;38:645–656.
44. Lee C, Staton RJ, Hintenlang DE, et al. Organ and effective doses in pediatric patients undergoing helical multislice computed tomography examination. *Med Phys*. 2007;34:1858–1873.
45. Li X, Samei E, Segars W, et al. Patient-specific dose estimation for pediatric chest CT. *Med Phys*. 2008;35:5821–5828.
46. Tzedakis A, Damilakis J, Perisinakis K, et al. Influence of *z* overscanning on normalized effective doses calculated for pediatric patients undergoing multidetector CT examinations. *Med Phys*. 2007;34:1163–1175.
47. Committee to Assess Health Risks from exposure to low levels of ionizing radiation. *Health Risks from Exposure to Low Levels of Ionizing Radiation. BEIR VII Phase 2*. Washington, DC: The National Academies Press; 2006:1–406.